Astronomy Reports, Vol. 47, No. 11, 2003, pp. 934–945. Translated from Astronomicheskiĭ Zhurnal, Vol. 80, No. 11, 2003, pp. 1013–1025.

Large-scale Dimmings Produced by Solar Coronal Mass Ejections According to SOHO/EIT Data in Four EUV Lines

I. M. Chertok and V. V. Grechnev

Institute of Terrestrial Magnetism, Ionosphere, and Radio Wave Propagation, Russian Academy of Sciences, Troitsk, Moscow oblast, 142190 Russia
Institute for Solar–Terrestrial Physics, P.O. Box 4026, Irkutsk, 664033 Russia

Received March 26, 2003; in final form, May 8, 2003

Abstract—SOHO/EIT data are used to analyze dimmings, or transient coronal holes (regions of reduced soft-X-ray and EUV emission), which are observed on the solar disk after halo-type coronal mass ejections (CMEs). Simultaneous observations in the 171 Å FeIX/X, 195 Å FeXII, and 284 Å FeIX coronal lines, which are sensitive to temperatures of $T_e \approx 1.2$, 1.5, and 2.0 MK, respectively, are considered, together with the 304 Å HeII transition-region line ($T_e \approx (0.02–0.08)$ MK). Difference images taken at intervals of six and twelve hours and compensated for solar rotation indicate that dimmings are normally strongly pronounced and have similar large-scale structures in the moderate-excitation-temperature 171 Å and 195 Å coronal lines, while the higher-temperature 284 Å line mainly display the deepest portions of the dimmings. In addition, clear dimmings with relatively small areas are visible in the 304 Å transition-region line during many CMEs, in particular, in regions adjacent to the source of the eruption. Moreover, dimmings in the transition region without coronal counterparts are observed during some events. These results suggest that the opening of magnetic-field lines and the resulting density reduction that occur during a CME can also involve cold plasma of the transition region. In addition, the effects of temperature variations cannot be ruled out for some dimming structures. © *2003 MAIK "Nauka/Interperiodica"*.

1. INTRODUCTION

Global restructuring and strong perturbations of the magnetic field during coronal mass ejections (CMEs) on the Sun are accompanied by large-scale phenomena, such as dimmings, coronal waves, post-eruptive arcades, etc. (see, e.g., the reviews [1–4] and references therein). Dimmings, or transient coronal holes [5–11], are regions of reduced soft X-ray and EUV emission with lifetimes of several hours to one and a half days. They are formed after the CME near the eruption center, for example, at the periphery of the pre-eruptive sigmoid structure, and can cover a large portion of the solar disk. Analyses of Yohkoh/SXT [12] and SOHO/EIT [13] heliograms suggest that dimmings should mainly be interpreted as a result of the complete or partial opening of the coronal magnetic fields in these structures, which results in the evacuation of material and a corresponding reduction in the intensity of their emission. Direct evidence for outflows from dimmings located near an eruption center was obtained in [10] based on the Doppler shifts of several lines recorded with the SOHO/CDS spectrometer [14].

A coronal wave is a emitting front that can fairly often be observed ahead of a developing dimming and can propagate from the eruption center at a speed of several hundred km/s [8, 15–22]. This wave is interpreted either as a MHD disturbance (shock wave)—a coronal analog of the chromospheric Moreton wave observable in Hα [23]—or as a result of the compression of plasma at the advancing boundary of the dimming—a region of opening magnetic-field lines [24, 25].

If the structure of the global solar magnetosphere is relatively simple (as is typical near the minimum of the activity cycle or during its growth phase, when only one active region is present on the solar disk), dimmings and coronal waves are more or less isotropic, and develop in a wide-angle sector symmetrically about the eruption source [8]. However, as is shown in [26], when the global solar magnetosphere is complex (as is typical near the cycle maximum, when several active regions, filaments, and other structures are observed on the disk), strongly anisotropic, channel-shaped ("channeled") dimmings can coexist with relatively compact dimmings adjacent to the eruption center. The channeled and compact dimmings have comparable contrasts, but the channeled dimmings stretch along several narrow, extended features (channels) and can span nearly the entire visible disk. In such cases, coronal waves are either not observed at all or are also

1063-7729/03/4711-0934$24.00

anisotropic and propagate within a restricted angular sector.

In some cases, so-called twin dimmings are observed, with the strongest intensity decreases occurring in two regions adjacent to the eruption center located symmetrically about the polarity-reversal line and the posteruptive arcade [8, 9]. Such twin dimmings are probably the bases of a large-scale twisted structure that exhibits eruptive behavior during the CME (see also [2, 27]). The post-eruptive arcade is formed when the strongly CME-disturbed magnetic field in a vast coronal region relaxes to an equilibrium state, reconnecting in extended current sheets high in the corona, and accompanied by prolonged energy release, particle acceleration (sometimes, to very high energies), and the formation of a system of rising loops [28].

To understand the nature of dimmings and coronal waves, it is important to analyze observations of these disturbances in various spectral lines and wavelength ranges. Almost all studies of currently known dimmings (and coronal waves) have been based on Yohkoh/SXT observations in soft X-rays corresponding to temperatures $T_e > 2.5$ MK or/and SOHO/EIT observations in the EUV FeXII line (195 Å), which are sensitive to coronal plasma at $T_e \approx 1.5$ MK [6–9, 11, 29]. These data are used precisely because they represent full-disk images obtained over fairly short time intervals—for example, usually 12 min for the 195 Å line. Meanwhile, full-disk SOHO/EIT heliograms are also observed in the 171 Å FeIX/X and 284 Å FeXV coronal lines excited at $T_e \approx 1.2$ and 2.0 MK, respectively, as well as with a 304 Å filter [13, 30], which includes the HeII transition-region line ($T_e \approx 0.02$–0.08 MK) and the far less intense SiXI coronal component ($T_e \approx 1.0$ MK). However, the use of 171, 284, and 304 Å heliograms is substantially limited by the large time interval between solar images, usually six hours. It is obvious that coronal waves cannot be studied using such heliograms; however, the situation is different for dimmings, since they have long lifetimes. Observations in the same four EUV lines with much higher time resolution are being carried out by the TRACE space observatory [31], but, like the SOHO/CDS spectrometer data [14], these data have been used little in studies of large-scale dimmings and coronal waves due to the restricted field of view of these instruments [10, 32, 33]. Thus far, the analysis of large-scale dimmings simultaneously either by Yohkoh/SXT soft X-ray data and 195 Å SOHO/EIT UV heliograms or by SOHO/EIT UV data in three coronal lines 171, 195, and 284 Å has been carried out for a few events only. Just these studies have revealed similarities between dimmings observed in coronal lines corresponding to different temperatures and in soft X-rays, and have demonstrated that the opening of magnetic structures and decreases in the plasma density in these structures play a more dominant role in dimmings than do temperature variations. To our knowledge, no observations of dimmings on the solar disk using a 304 Å filter have been analyzed to date. In [36], 304-Å heliograms were used to analyze only one eruptive event at the limb.

We analyze dimmings here using data for all four SOHO/EIT wavelengths, including the band containing the HeII transition-region line. This requires special methodological approaches, which are described in Section 2. Four events are used in Section 3 as examples to illustrate the multi-temperature properties of dimmings observed in the FeIX/X, FeXII, and FeXV coronal lines and the HeII transition-region line. We discuss our results in Section 4.

2. METHODOLOGICAL NOTES

In the standard SOHO/EIT observing regime, heliograms in a $45' \times 45'$ field of view with a 1024×1024 frame and $2.6''$ pixels are recorded once every 12 minutes in the high-priority 195 Å line and four times each day (at about 1, 7, 13, and 19 UT) in the 171, 284, and 304 Å lines [30]. Only during rare and relatively short special programs is the twelve-minute regime implemented for lines other than the 195 Å line. In such cases, however, data for the analysis of some particular event in all four lines remain limited and nonuniform. Moreover, the probability of recording major eruptive events during such special, short-term programs is not high. At the same time, detailed analyses of the development of dimmings and coronal waves in lines other than the high-priority line are obviously of considerable interest, and should be the subject of careful studies. We have used here data of standard SOHO/EIT observations. The corresponding FITS files are available in the EIT catalog at http://umbra.nascom.nasa.gov/eit/eit-catalog.html.

Events in which a CME and the main stages of the development of dimmings occur during a six-hour interval between observations in the 171, 284, and 304 Å lines are the most suitable for the desired analysis, provided that no other major eruptive events take place during this interval. The analysis in each of the four lines includes comparisons of heliograms taken before and after the event. The dimmings are most pronounced in difference images obtained by subtracting the pre-event heliogram from the corresponding heliogram taken during or after the event.

In such images, dimmings appear as dark features with reduced intensity. However, a simple subtraction of two images, especially over a six-hour interval, will inevitably give rise to artifactual light and dark features (spurious dimmings), since the solar rotation leads to the displacement of features on the disk. To avoid such effects, we employed an IDL procedure before the subtraction to compensate for the solar rotation, as is done in [26]—the images at each wavelength are all rotated to a single reference position, usually corresponding to a time before the event.

In particular, this procedure for rotating (aligning) the images made it possible to analyze events that culminated near one of the observational times in the 171, 284, and 304 Å lines (i.e., 1, 7, 13, or 19 UT), as long as the events were isolated. In such cases, the difference images were constructed using frames taken twelve hours apart, and both the reference and subtracted frames were rotated to the time of a central frame taken during the event; i.e., they were shifted by six hours. For example, if the event occurred near 13 UT, the difference images were obtained from the 7 UT and 19 UT heliograms, which were first rotated to 13 UT.

For adequate comparison of dimmings in all four lines, rotated (aligned) images of six-hour or twelve-hour intervals were formed not only at the 171, 284, and 304 Å wavelengths, but also in the 195 Å line. The much more detailed twelve-minute data at this wavelength and the running- and fixed-difference images obtained from them after compensation for the solar rotation were used to gain information on the development of dimmings and accompanying phenomena. The running difference images are produced by subtracting the preceding heliogram from each current heliogram, while the fixed-difference images are created by subtracting the same reference image of the disk (usually obtained before the event) from all subsequent heliograms. The running difference images emphasize changes in the brightness, location, and structure of sources that have appeared during the interval between successive frames. Changes that have occurred during the event, including dimmings, are clearly visible in the fixed-difference images (naturally, relative to the chosen pre-event reference frame). Obviously, in forming difference images over a six-hour interval, there is no reason to associate all brightness variations on the disk with the eruptive event considered, even if it is an isolated event, since weak independent activity is almost constantly present in other regions of the disk, and also manifests itself in the difference heliograms.

As in [26], the difference images were formed in a restricted intensity range to make the dimmings better defined against the background of other structures. As a result, the brightest sources (in particular, those arising during a flare and in the posteruptive phase) are usually saturated. Naturally, the outlines and some structural details of the dimmings vary to some extent, depending on the choice of intensity range. One more remark concerns Grid-like patterns—systems of periodic vertical and horizontal strips—that are fairly common in the original SOHO/EIT images and have an instrumental origin [13, 30]. In the rotated difference images, the horizontal strips disappear but the vertical strips are enhanced inside the disk, especially if the heliograms are rotated by a large angle, corresponding to a six-hour interval, as in this case.

This technique for the formation of six-hour or twelve-hour SOHO/EIT difference images compensated for solar rotation enabled us to analyze simultaneous manifestations of dimmings in the four EUV lines.

3. ANALYSIS OF PARTICULAR EVENTS

We employed the above technique to analyze several dozen eruptive events occurring in 1997–2002, mainly related to halo CMEs recorded by the SOHO/LASCO coronagraph [37] in which the source of eruption was located in the central zone of the visible disk. Some of these events such as the rotated six-hour or twelve-hour difference images in the 171, 195, 284, and 304 Å lines, detailed data on the development of accompanying disturbances observed at 195 Å presented in the form of JAVA computer movies containing running- and fixed-difference images, and other illustrations, including data on CMEs and the time profiles and relative depths of dimmings, can be found at http://helios.izmiran.troitsk.ru/lars/Chertok/Dimming/general.html.

To demonstrate the multi-wavelength characteristics of the dimmings, we consider below the same three events described by us in [26] in the context of studies of channeled dimmings at 195 Å, and supplemented them by another event with well-defined dimmings in the transition-region line. Thus, our study can be considered as a continuation of [26], where information on the first three events is given in more detail; in particular, there we describe the development of dimmings in the 195 Å line based on twelve-minute heliograms. For each of the events considered, in addition to the rotated difference images showing the dimmings in all four wavebands arranged in order of increasing temperature, the corresponding figures of this section include the original 284 and 304 Å heliograms illustrating the background against which the eruption took place.

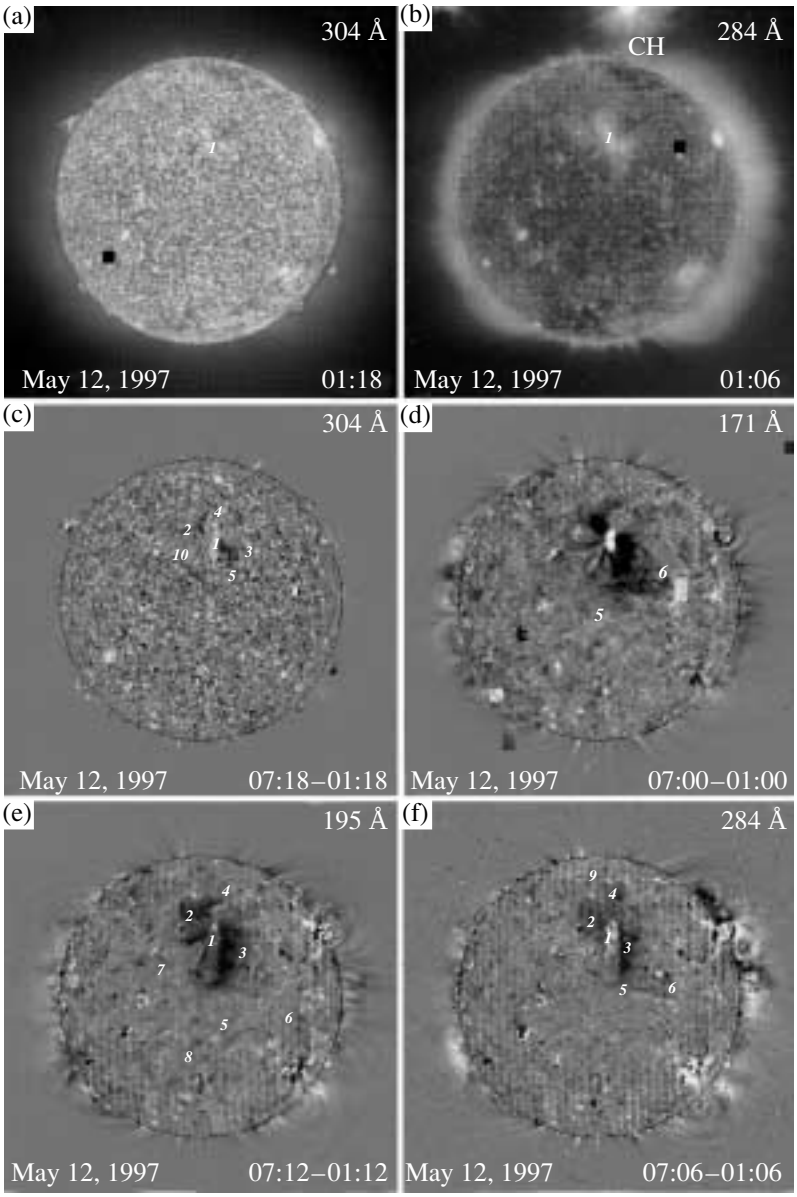

Fig. 1. Event of May 12, 1997: (a), (b) pre-event SOHO/EIT heliograms in the 304 and 284 Å lines and (c)–(f) rotated six-hour difference images in the 304, 171, 195, and 284 Å lines, illustrating the location and structure of dimmings in the transition region and corona.

3.1. Event of May 12, 1997

The characteristics of the halo CME and related quasi-isotropic large-scale disturbances in this well-known eruptive event have been analyzed many times [3, 8, 26, 27, 38]. The overall similarity in the locations and shapes of the deepest dimmings near the eruption center in the 171, 195, and 284 Å coronal lines was demonstrated in [8] using the original (not difference) SOHO/EIT heliograms. It is interesting to analyze the manifestation of the dimmings of this event in the six-hour difference heliograms, using both the coronal lines and the 304 Å transition-region line.

The eruption source was located in AR 8038 (region *1* in Fig. 1), which was observed in the central zone of the northern half of the disk (N21, W09) and was essentially the only active region on the visible hemisphere (Figs. 1a, 1b); the event as a whole was associated with a long-lived flare of class 1F/C1.3 with its maximum near 04:50 UT. The CME recorded by the SOHO LASCO coronagraph was classified as a full halo emitting everywhere around the occulting disk, but its brightness was maximum over the eastern, western, and northern limb sectors [38].

According to the 195 Å observations, the mod-

erately deep dimmings and coronal wave (in this case, under the conditions of a relatively simple global solar magnetosphere) were quasi-isotropic and covered the visible disk almost entirely [3, 8, 26]. Under the chosen restriction of the intensity range the deepest dimmings can be seen in the difference heliogram between 07 and 01 UT (Fig. 1e), first of all, as two darkened regions with similar sizes and shapes (twin dimmings) situated symmetrically about the eruption center, northeast and southwest of the bright, compact posteruptive arcade 1. In addition to the main dimmings 2 and 3 directly joining to the posteruptive arcade, the intensity is also considerably reduced in the fairly extended branches 2-4 and 3-5, which emerge from these dimmings and stretch toward the northern polar coronal hole (CH) and the heliographic equator, respectively. Branch 3-5 of the dimming broadens near its southern end and has a faint westward extension along the equator, to point 6. Two other narrow dimming branches, 1-7 and 1-8, originate from the eastern edge and southern end of the posteruptive arcade, with the southern branch 1-8 even intersecting the heliographic equator.

Similar dimmings can be seen in the corresponding 171 Å heliogram (Fig. 1d); i.e., at a somewhat lower temperature of the coronal plasma. Some differences can be noted in the southern branch of the dimming, which splits in region *5*, while its westward equatorial continuation 5-6 appears as two parallel strips with a more pronounced darkening (deeper dimming) than in the 195 Å line. Another difference is the lack of the transequatorial dimming branch 1-8 observed in the 195 Å line.

The twin structure of the main dimmings 2-4 and 3-5 is also reproduced in the high-temperature 284 Å coronal line (Fig. 1f). Of the dimming branches, the southern component of the westward, near-equatorial dark strip 5-6 is also visible here. In addition to showing the dimmings, the emitting chain 1-9 is most pronounced in this line; it has developed by this time (07:06 UT) along the western edge of the northeastern dimming 2-4, from the posteruptive arcade to the southern boundary of the northern polar coronal hole. As is shown in [8] and follows from analyses of the available heliograms (including difference heliograms), within the next two to twelve hours, this chain had stretched over the entire southern boundary of the coronal hole, and was observed in the 171, 284, and 304 Å lines as well as in the 195 Å line. As in other similar cases [39], the formation of this chain seems to result in connection with energy released due to the interaction between the open field lines of the coronal hole and large-scale magnetic structures involved in the CME process.

It is important that manifestations of dimmings are also pronounced in the six-hour difference heliogram taken in the 304 Å transition-region line (Fig. 1c). Here, some analogs of the main coronal twin dimmings, 1-2-4 and 1-3-5, are observed on either side of the posteruptive arcade. The considerably smaller width and extent of the dimmings in the 304-Å line, as well as their locations, suggest that the transition region is reached by the deepest, central regions of the coronal dimmings. Moreover, some dimming fragments that are not visible in the coronal lines are revealed in the 304 Å line, such as the branch 2-10 that originates from point 2 toward the southwest. It will become clear below that, with some variations, such situations are also typical of other eruptive events.

Note that, as seen from the rotated difference heliograms taken at even longer time intervals, the twin dimmings described above and the brightening along the southern boundary of the northern polar coronal hole recorded in the three coronal lines and the transition-region line were observed over at least 15 hours, until 19 UT, and largely preserved their spatial structure during this time.

3.2. Event of January 18, 2000

In contrast to the preceding event, this eruptive event occurred in a fairly complex global solar magnetosphere, when several active centers, filaments, and coronal holes were observed on the disk (Figs. 2a, 2b). In particular, it included a prolonged class 1N/M3.9 flare with its maximum at 17:27 UT in the southeastern active region AR 8831 (S19 E11; region 1 in Fig. 2) and a well-defined halo CME, which initially developed over the eastern limb and subsequently extended over all position angles. Note that the eruptive southeastern prominence seen in the 304 Å pre-event heliogram (Fig. 2a) and its counterpart in the 304 and 171 Å difference heliograms (Figs. 2c, 2d) are associated with the preceding near-limb activity.

As is shown in [26] and can be seen from the six-hour difference image in the 195 Å line (Fig. 2e), the corresponding dimmings displayed an anisotropic structure in the form of extended, channeled transequatorial features. An annular dimming is visible in the immediate vicinity of the eruption center and posteruptive arcade 1, whose deepest parts are the northern and southeastern elements 2 and 3. The latter feature is connected with active center 4, located in the northern half of the disk near the central meridian, by a pronounced, narrow transequatorial dimming strip, and has a westward extension 4-5. The other eastern transequatorial channeled dimming 6-7, which is fragmentary in places and less intense,

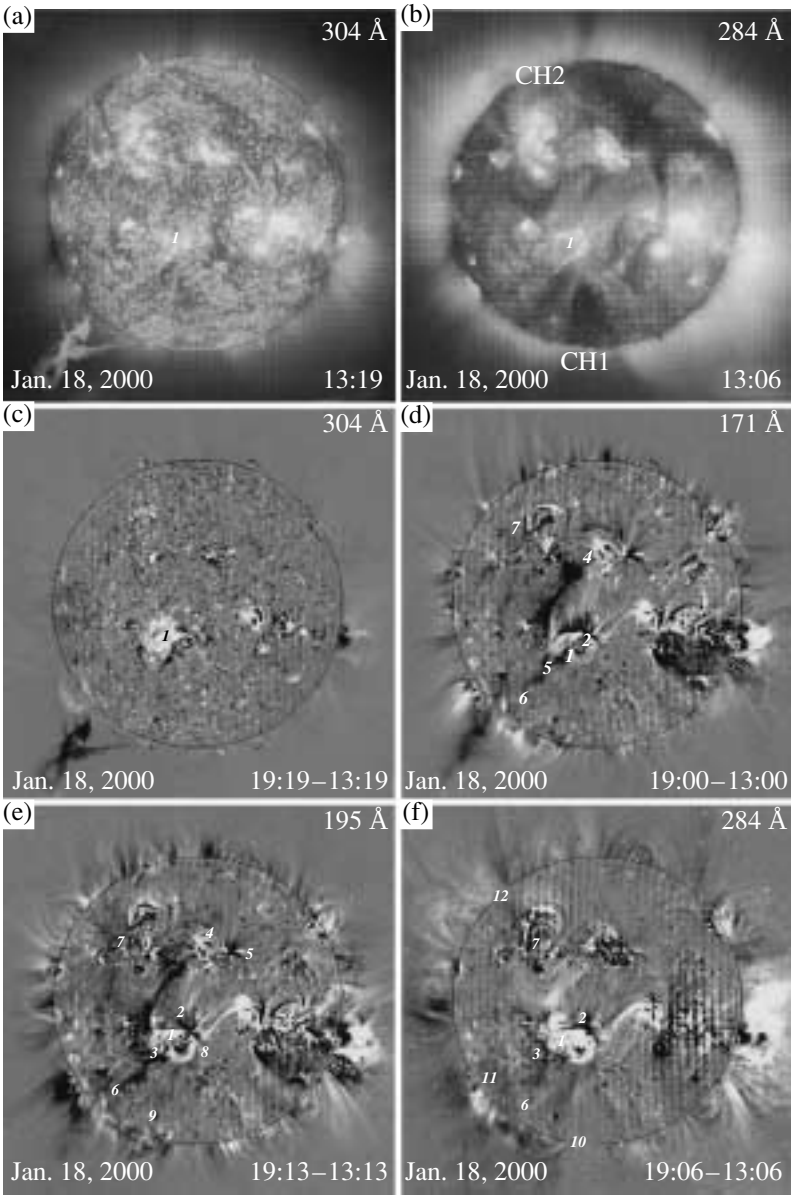

Fig. 2. Same as Fig. 1 for the event of January 18, 2000.

emerges from the southeastern dimming loop 3-6 and stretches toward the active region in the northeastern quadrant. Some of the other dimmings described in [26] are also visible in this difference image, in particular, the relatively faint dimming 8-9, which partially borders the edge of a southern polar coronal hole observed, e.g., in the 284 Å line (Fig. 2b). The relationship between this eruptive event and the dimmings observed in the southwestern quadrant remains unclear.

The main dimmings, including elements 2 and 3 joining to the eruption center, and both channeled transequatorial structures, 6-3-4 and 6-7, are also observed in the lower-temperature 171 Å line (Fig. 2d).

However, substantial differences are visible in the highest-temperature 284 Å line (Fig. 2d), which are important for our understanding of the origin of dimmings. In this case, they are mainly associated with the transequatorial dimmings noted above. The eastern dimming branch that goes toward the northeastern active complex 7 is almost indistinguishable, while an appreciable brightening is present in the transequatorial structure 1-4 between the eruption center and the northern active region, instead of a deep dimming. The brightening also affects the entire equator-facing loop system, which connects active

centers 4 and 7 of the northern hemisphere; i.e., a considerable portion of the space between the eastern and western transequatorial dimming branches seen at 171 and 195 Å. At the same time, in the 284 Å line, the deepest dimmings 2 and 3 adjoining to the eruption center and the southeastern dimming loop 3-6 are similar to those observed at 171 and 195 Å. In addition, at 284 Å, there is some intensity decrease (i.e., a weak dimming) localized generally within the southeastern sector 1-10-11-1, although the eastern edge of the sector, which coincides with the eastern boundary of the southern polar coronal hole CH1, seems to be slightly brightened, as are some other narrow structures inside the sector. The dimming 7-12, which stretches toward the southeastern limb along the narrow CH2, is more pronounced at 284 Å than in the other lines.

Transition-region manifestations of dimmings in the 304 Å line are not significant in this event, as can be seen from the corresponding difference heliogram (Fig. 2c). Only dimming fragments with relatively small areas can be distinguished in the coronal lines around the eruption center 1. In particular, there are well-defined dimming fragments and narrow loop structures east, south, and west of the eruption center.

3.3. Event of February 17, 2000

This event occurred one rotation after the preceding one (Section 3.2) at nearly the same site on the solar surface; i.e., in the presence of a similarly complex global solar magnetosphere. It developed against the background of two sympathetic flares of classes M2.5/1B and M1.3/2N that occurred in the nearby southern active regions AR 8869 and AR 8872 (S25 W16 and S29 E07; regions 1 and 2 in Fig. 3) and reached their maxima in soft X-rays at 18:52 and 20:35 UT, respectively [40]. According to the SOHO/LASCO coronagraph data, the first signs of a CME were observed over the southwestern limb at 19:31 UT, and an almost symmetric halo CME developed around the entire occulting disk after 20:06 UT.

Since the event developed most intensely near 19 UT, the frames taken at that time cannot be used to construct the difference images in the four lines. For this reason, the rotated difference heliograms shown in Figs. 3c–3f were obtained using a twelve-hour interval, as the difference between the frames of 13 UT on February 17 and 1 UT on February 18, after they were first rotated to 19 UT on February 17 at each wavelength. Analysis of these heliograms confirms the conclusion drawn earlier based on detailed data in the 195 Å line [26] that the dimmings that accompanied this event were global, mainly channeled, reflected the magnetic coupling between all the active regions situated in the central sector of the disk on both sides of the equator, and covered the entire space between these regions (see also [40]).

This dimming structure is also visible in the twelve-hour 195 Å difference heliogram (Fig. 3e). Some dimmings here abut on the western eruption center 1. One or two dimming strips 3-4 and the dimming 5 to the north of these emerge from this center toward the west. Two dimming arcs branch at point 3, curving around the eruption center 1 from the south and stretching toward the eastern dimming 6. In turn, this last dimming is connected with the eastern eruption center 2 by the narrow channel 6-7. This center is surrounded by the dimming 7-8 from the north and the well-defined dimming loop 9 from the south. The transequatorial dimming channel 7-10-11 goes from the eruption center 2 through the knot 10 toward the northern active region. The connection between these regions and those to the east of the central meridian is also indicated by a number of dimming channels, such as the southern horizontal strips 8-12 and 10-13-14-15, the northern horizontal strip 16-17-11, and the vertical dimmings 13-17 and 14-16 connecting these strips. The northern horizontal strip 16-17-11 extends in the west to the northwestern region 18—the neighborhood of a small coronal hole. Relatively faint but clearly visible transequatorial dimmings directly connect the western eruption center 1 with the northern region 11 and the northwestern region 18. On the whole, the global system of channeled dimmings described here reflects the fact that the magnetic structures of the entire circular central sector of the disk were involved in the eruption process. As is noted in [26], the positions and configurations of most channeled dimmings correspond to elements of the annular system of emitting UV chains that was visible in the 195 Å line before the event in the same central sector of the disk. It is probably the eruption of precisely these magnetic structures that determined the quasi-symmetric annular shape of the halo CME observed in this event.

A very similar dimming system can also be seen in the corresponding 171 Å heliogram (Fig. 3d). One small difference is the somewhat weaker manifestation of the dimmings between the western eruption center 1 and the northern regions 11 and 18. On the other hand, the knot 13 and the main eastern and northeastern channels aligned with the curve 15-14-16-17-11 are more pronounced.

A different situation with regard to dimmings is observed in the high-temperature 284 Å line. The corresponding difference heliogram (Fig. 3f) displays all the main dimmings adjoining to the eruption

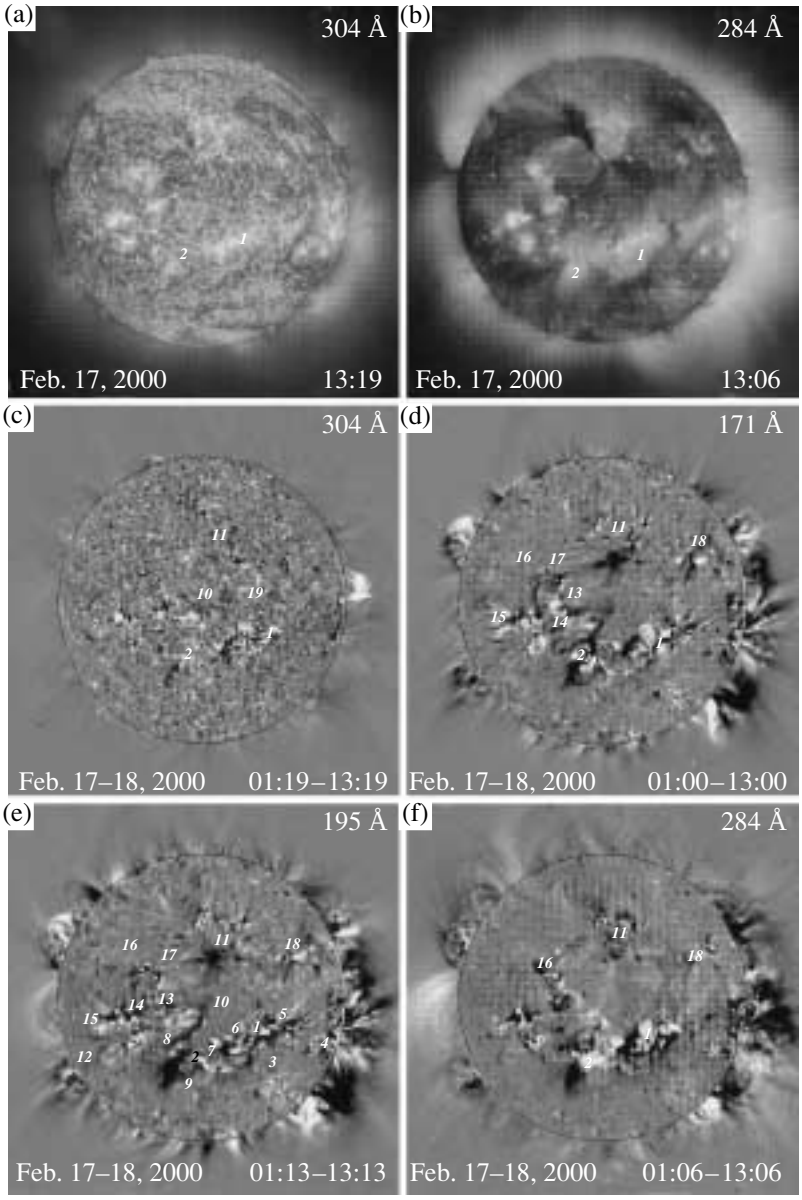

Fig. 3. Same as Fig. 1 for the event of February 17, 2000. The rotated difference images (c)–(f) were obtained over the twelve-hour interval between 13 UT and 1 UT on February 18, 2000; all the heliograms were rotated to 19 UT on February 17, 2000.

centers 1 and 2, and, as in the other two coronal lines, the pattern of the channeled dimmings generally reflects the connections between the active regions in the central sector of the disk. In this heliogram, some eastern transequatorial dimmings are less pronounced, while western dimmings, e.g., in the strip 1-18, are slightly more intense. However, no analogs of the dimming knot 10 and the entire transequatorial dimming between the eastern eruption center 2 and the northern active region 11 are observed at 284 Å (Figs. 3d, 3e). On the contrary, a weak brightening is present instead of the dimming, while a slight intensity decrease is observed west of this structure, up to the strip 1-18. Another brighter transequatorial structure stretches from the zone between the eruption centers 1 and 2 toward the northwestern dimming region 16.

As in the preceding events, fragments of the deepest dimmings are mainly visible in the 304 Å transition-region line (Fig. 3c), in particular, near the eruption centers 1 and 2. The dimming knot 10 on the line between regions 2 and 11 also stands out. It is noteworthy that a new dimming knot, 19, which is not observed in the coronal lines, appears slightly to the west and north of the knot 10. It is possible to see on a computer screen and in high-quality prints

of the heliogram (Fig. 3c) that the knot 19 is linked by a weak dimming with the northern active region.

3.4. Event of April 29, 1998

This eruptive event included a long-lived flare of class 3B/M6.8 in the southeastern AR 8210 (S21 E03), which had its soft-X-ray maximum at 16:37 UT. It is noteworthy that the corresponding CME appeared as a two-component halo with a white-light maximum over the northeastern and southwestern sectors of the limb. During the event, AR 8210 (region 1 in Fig. 4) was essentially the only active region on the disk, but it was adjacent to a large transequatorial coronal hole, CH1 (Fig. 4b), which occupied nearly the entire central zone of the disk, and two other, much smaller, coronal holes CH2 and CH3 located between the eruption source 1 and the eastern limb. The unusual appearance of the CME [35] and the peculiar manifestations of the dimmings in the 304 Å line (see below) were apparently related to these features of the global solar magnetosphere.

Analysis of running-difference and fixed-difference images and movies obtained using the available 195-Å data in intervals of 12-16 min shows additional features of this event (see the web site noted at the beginning of Section 3). A well-defined coronal wave propagated from the eruption center in two angular sectors—toward the northeastern limb and westward; i.e., through CH1. (Such propagation of a coronal wave within a coronal hole is apparently rarely observed, and deserves special consideration in a separate study.) Like the first sector of the coronal wave, the main dimmings in 195 Å developed in the direction of the northeastern limb. This can also be seen in the rotated six-hour difference heliogram (Fig. 4e). The deep transequatorial dimming 2-3, which formed in the immediate vicinity of CH1, extends toward northern region 3 and joins with the eastern meridional dimming 4-5. The narrow dimming 6-7 curves around the eruption center 1 from the south; this dimming also has a number of even narrower extensions in the eastern and northeastern directions, in particular, toward point 4. Weak manifestations of dimmings and fragmentary brightenings are also observed along the southern (8-9) and northern (3-10) boundaries of CH1. A distinct but small intensity reduction also covers the entire space of CH1, and several arc-like channels stand out against this background, in particular, between points 6 and 9. A similar slight intensity reduction is probably present to the east of the dimming 7-4-5.

As usual, an overall similar dimming structure is also observed in the 171 Å line (Fig. 4d). Minor differences from the 195 Å pattern include the fact that dimming 2 is somewhat broadened in the longitudinal direction in the immediate vicinity of the eruption center 1, and only individual fragments replace the eastern meridional dimming 4-5 (Fig. 4e), especially its northern part. In addition, the small-area dimmings 11 near the northern boundary of CH1 and some dimmings within CH1, including the arc-like structure 2–9, are enhanced.

In this event, the main dimming 2 and its transequatorial extension toward the northeastern region 3 are also present, although somewhat weaker, in the difference heliogram taken in the high-temperature 284 Å coronal line (Fig. 4f). The Yohkoh/SXT data confirm the tendency for the dimming 2-3 to weaken with increasing temperature: as shown in [35], dimming 2 is almost invisible in soft X-rays, i.e., at even higher plasma temperatures, $T_e > 2.5$ MK. The eastern meridional dimming 4-5, which is most pronounced in the 195 Å line (Fig. 4a) is likewise only weakly manifest at 284 Å. At the same time, the dimming 6-7-4 passing to the south and southeast of the edge of the posteruptive arcade 1 is visible as clearly as in the other two coronal lines. Intensity variations corresponding to CH1 can also be seen in 284 Å. The faint chains 3-10 are observed along the northern boundary of CH1, which adjoins on narrow, faint dimming structures. Similar structures are also localized within CH1 (6-9) and along its western boundary (9-10).

In contrast to the three events described above, in this case, the largest-area dimmings can be distinguished in the difference heliogram in the 304 Å transition-region line (Fig. 4c). Not only are analogs of the northern (2) and southern (6-7) coronal dimmings clearly visible near the eruption center 1, but an intensity decrease with appreciable amplitude and area (i.e., a transient coronal hole) can also be seen in the southern part of CH1. A deep dimming starts from the broadened eastern end (6) of the southern dimming, covers an extensive portion of CH1 stretching westward to point 12, then bends and extends toward the southeast to point 13, located near the southern boundary of CH1. This seems to imply that the CME-induced restructuring of the magnetic field (opening of the field lines) has also affected the underlying transition-region plasma in the southern portion of CH1 and in the space between the eruption center 1 and CH1. As can be seen in Fig. 4c, this process was also accompanied by the formation of a emitting chain along the southern boundary of dimming 6. A similar emitting structure is also present at the eastern edge of dimming 2.

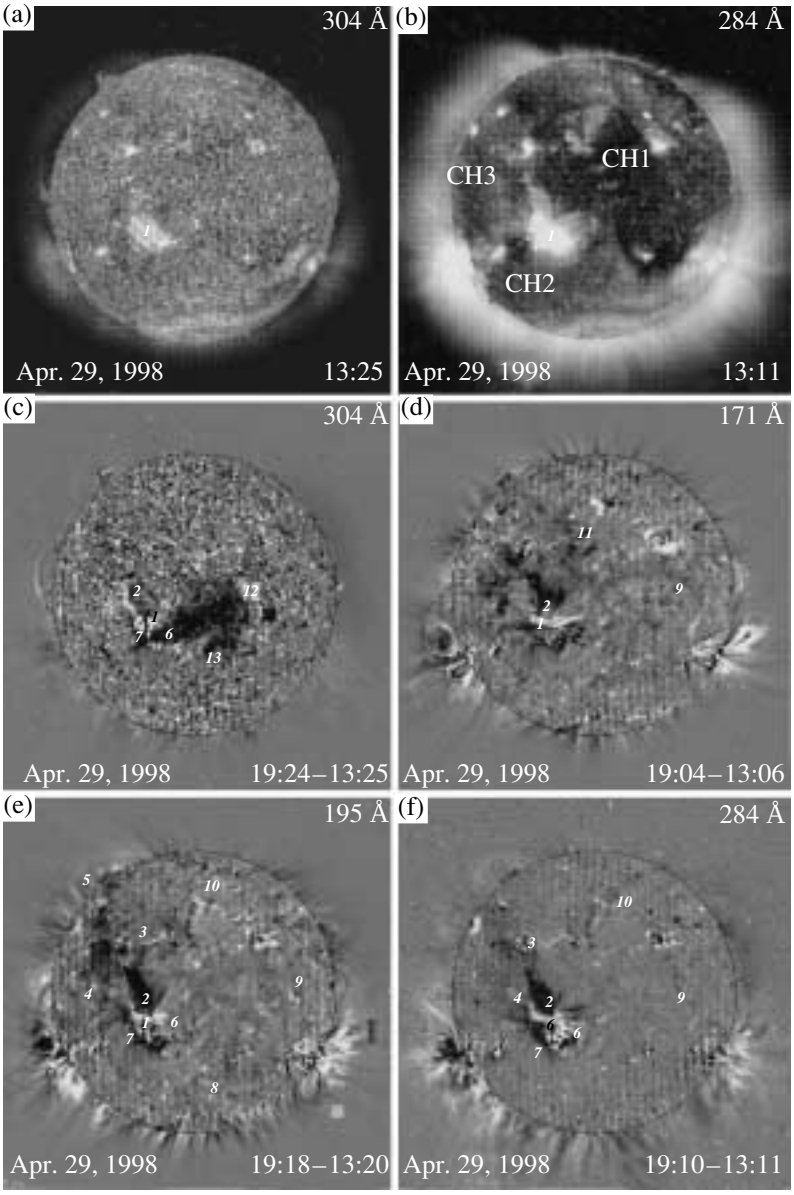

Fig. 4. Same as Fig. 1 for the event of April 29, 1998.

4. DISCUSSION AND CONCLUSION

The reduction of SOHO/EIT UV heliograms with compensation for the rotation of the solar disk has enabled us to construct rotated difference images over six-hour (and 12-hour, when required) intervals, and to study CME-produced dimmings (transient coronal holes) simultaneously in three coronal lines (171, 195, and 284 Å) and a transition-region line (304 Å). This was also possible because the lifetimes of major dimmings normally exceed these time intervals.

Our analysis provides additional evidence that, at least in the three coronal lines, the dimming disturbances and transient brightenings produced by major CMEs are essentially global and span the space between well-separated activity centers that may be located on both sides of the heliographic equator. This means that a large portion of the global solar magnetosphere is involved in the eruption process. Structures directly linked to the eruption center by magnetic fields appear to be primarily involved in this process [41].

The data obtained in all four lines also confirm the conclusion obtained earlier based on a detailed analysis of 195 Å data [26] that, when the global solar magnetosphere is complex and several active-region filaments, coronal holes, etc. are present on the solar disk, many dimmings are anisotropic, and can be observed as narrow, extended channels.

In many cases, the reduction of the EUV intensity of the dimmings in all four lines is comparable to that at 195 Å and, according to the estimates of [3, 9, 26], can reach several tens of percent.

Well-defined dimmings adjacent to the eruption center are recorded in all four lines. They have nearly the same shapes and locations in the three coronal lines, while only the deepest fragments of such dimmings can normally be seen in the transition-region line, rather than the entire coronal dimming area. This, firstly, supports the previous conclusion of [3, 8, 9] that such dimmings result from a CME-related partial or complete opening of field lines in the corresponding magnetic structures and the evacuation of plasma from them, and, secondly, suggests that this process involves not only the coronal plasma but, to some extent, the transition-region plasma as well. We should bear in mind that the fragmentary dimmings observed in the immediate neighborhood of eruption centers (or active regions) at 304 Å may be partially due to a reduction in the emission of the SiXI coronal line, which is also recorded by the 304 Å filter [13, 30].

Channeled dimmings, especially transequatorial ones, are manifested most clearly and in very similar ways in the 171 and 195 Å coronal lines, which have moderate excitation temperatures. The events of January 18 and February 17–18, 2000 (Sections 3.2 and 3.3) show that a brightening in pre-existing loop structures is observed at the locations of some transequatorial dimmings in the high-temperature 284 Å line. This suggests that the reduction in EUV intensity of such structures in some lines and its enhancement in others may be initiated by changes in the plasma temperature—for example, by heating due to CME-related thermal or MHD disturbances. The above considerations do not mean that transequatorial dimmings cannot be observed at all in the high-temperature UV line, or even in soft X-rays. Examples of transequatorial dimmings in the 284 Å line were indicated in our description of the events of February 17–18, 2000 (Section 3.3), and April 29, 1998 (Section 3.4), and examples of observations of such dimmings in soft X-rays are given in [21, 42] (based on Yohkoh/SXT data). The analysis of numerous transequatorial loops presented in [43] shows that CME-related variations in the EUV (195 Å) and soft-X-ray intensities can be manifested as dimmings in some cases and as loop brightenings in others.

Our analysis of heliograms in the 304 Å transition-region line reveals dimmings invisible in the coronal lines that appear far from the active region. In some cases (the event of February 17–18, 2000; Section 3.3), these are dimming elements with relatively small areas and intensity reductions, while in others (the event of April 29, 1998; Section 3.4), they are clearly defined dimmings occupying a considerable portion of a large coronal hole adjacent to the eruption center. Such dimmings can arise, in particular, as a result of the heating of the transition-region plasma (sinking of the corona) during a CME. Another possibility is the opening of field lines and outflow of material from originally closed, low-lying structures in the transition region. In the case of the event of April 29, 1998, this second possibility implies that the transition-region plasma is directly involved in the eruption process, so that a continuation of a substantial portion of the existing coronal hole is formed at transition-region altitudes; i.e., a transient "hole" develops in the transition region.

As noted in Section 3, brightenings in the form of elongated emitting chains are observed during some events after a CME, at the boundaries of some dimmings or coronal holes in all four lines [8, 39]. Their origin is most likely related to the energy released due to reconnection during the interaction of evolving open magnetic structures involved in the CME with neighboring closed magnetic fields.

In conclusion, we emphasize again that our analysis of dimmings was based on rotated six-hour and 12-hour SOHO/EIT difference heliograms, obviously, this should be considered as the first step only. A more detailed analysis of CME-related disturbances (especially coronal waves) in various spectral lines requires much higher time resolution, reaching tens of seconds or several minutes. Such observations—in the same four lines—are being conducted on the TRACE (which has a restricted field of view) [31, 33] and CORONAS F (which can obtain full-disk images) [44, 45] space observatories.

ACKNOWLEDGMENTS

The authors are grateful to the SOHO/EIT team for the data used in our analysis. This work was supported by the Russian Foundation for Basic Research (project nos. 03-02-16049 and 03-02-16591) and partially by the Ministry of Industry, Science, and Technology of the Russian Federation.

REFERENCES

1. D. F. Webb, J. Atmos. Sol.-Terr. Phys. **62**, 1415 (2000).
2. A. C. Sterling, J. Atmos. Sol.-Terr. Phys. **62**, 1427 (2000).
3. N. Gopalswamy and B. J. Thompson, J. Atmos. Sol.-Terr. Phys. **62**, 1458 (2000).
4. H. S. Hudson and E. W. Cliver, J. Geophys. Res. **106**, 25199 (2001).
5. D. M. Rust, Space Sci. Rev. **34**, 21 (1983).

6. A. C. Sterling and H. S. Hudson, Astrophys. J. Lett. **491**, L55 (1997).
7. H. S. Hudson and D. F. Webb, in *Coronal Mass Ejections,* Ed. by N. Crooker, J. Joselyn, and J. Feynman (1997), AGU Geophys. Monogr. Ser., No. 99, p. 27.
8. B. J. Thompson, S. P. Plunkett, J. B. Gurman, *et al.*, Geophys. Res. Lett. **25**, 2465 (1998).
9. D. M. Zarro, A. C. Sterling, B. J. Thompson, *et al.*, Astrophys. J. Lett. **520**, L139 (1999).
10. L. K. Harra and A. C. Sterling, Astrophys. J. Lett. **561**, L215 (2001).
11. S. W. Kahler and H. S. Hudson, J. Geophys. Res. **106**, 29239 (2001).
12. S. Tsuneta, L. Acton, M. Bruner, *et al.*, Solar Phys. **136**, 37 (1991).
13. J.-P. Delaboudiniere, G. E. Artzner, J. Brunaud, *et al.*, Solar Phys. **162**, 291 (1995).
14. R. A. Harrison, E. C. Sawyer, and M. K. Carter, Solar Phys. **162**, 233 (1995).
15. B. J. Thompson, J. B. Gurman, W. M. Neupert, *et al.*, Astrophys. J. Lett. **517**, L151 (1999).
16. A. Klassen, H. Aurass, G. Mann, *et al.*, Astron. Astrophys. **141**, 357 (2000).
17. B. J. Thompson, B. Reynolds, H. Aurass, *et al.*, Solar Phys. **193**, 161 (2000).
18. A. Warmuth, B. Vrsnak, H. Aurass, *et al.*, Astrophys. J. Lett. **560**, L105 (2001).
19. D. A. Biesecker, D. C. Myers, B. J. Thompson, *et al.*, Astrophys. J. **569**, 1009 (2002).
20. N. Narukage, H. S. Hudson, T. Morimoto, *et al.*, Astrophys. J. Lett. **572**, L109 (2002).
21. J. L. Khan and H. Aurass, Astron. Astrophys. **383**, 1018 (2002).
22. H. S. Hudson, J. L. Khan, J. R. Lemen, *et al.*, Solar Phys. **212**, 121 (2003).
23. G. E. Moreton and H. E. Ramsey, Publ. Astron. Soc. Pac. **72**, 357 (1960).
24. C. Delannee and G. Aulanier, Solar Phys. **190**, 107 (1999).
25. C. Delannee, Astrophys. J. **545**, 512 (2001).
26. I. M. Chertok and V. V. Grechnev, Astron. Zh. **80**, 162 (2003) [Astron. Rep. **47**, 139 (2003)].
27. D. F. Webb, R. P. Lepping, L. Burlaga, *et al.*, J. Geophys. Res. **105**, 27251 (2000).
28. I. M. Chertok, in *Proceedings of the Fifth SOHO Workshop*; ESA SP **404**, 269 (1997).
29. S. Pohjolainen, D. Maia, M. Pick, *et al.*, Astrophys. J. **556**, 421 (2001).
30. D. Moses, F. Clette, J.-P. Delaboudinire, *et al.*, Solar Phys. **175**, 571 (1997).
31. B. N. Handy, L. W. Acton, C. C. Kankelborg, *et al.*, Solar Phys. **187**, 229 (1999).
32. M. J. Wills-Davey and B. J. Thompson, Solar Phys. **190**, 467 (1999).
33. L. K. Harra and A. C. Sterling, Astrophys. J. **587**, 429 (2003).
34. A. C. Sterling, H. S. Hudson, B. J. Thompson, *et al.*, Astrophys. J. **532**, 628 (2000).
35. H. Wang, P. R. Goode, C. Denker, *et al.*, Astrophys. J. **536**, 971 (2000).
36. C. Delannee, J. Atmos. Sol.-Terr. Phys. **62**, 1471 (2000).
37. G. E. Brueckner, R. A. Howard, M. J. Koomen, *et al.*, Solar Phys. **162**, 357 (1995).
38. S. P. Plunkett, B. J. Thompson, R. A. Howard, *et al.*, Geophys. Res. Lett. **25**, 2477 (1998).
39. I. M. Chertok, Solar Phys. **198**, 367 (2001).
40. H. Wang, V. Yurchyshyn, J. Chae, *et al.*, Astrophys. J. **559**, 1171 (2001).
41. T. Wang, Y. Yan, J. Wang, *et al.*, Astrophys. J. **572**, 580 (2002).
42. J. I. Khan and H. S. Hudson, Geophys. Res. Lett. **27**, 1083 (2000).
43. A. Glover, L. K. Harra, S. A. Matthews, and C. A. Foley, Astron. Astrophys. **400**, 759 (2003).
44. V. N. Oraevsky and I. I. Sobelman, Pis'ma Astron. Zh. **28**, 457 (2002) [Astron. Lett. **28**, 401 (2002)].
45. I. A. Zhitnik, O. I. Bougaenko, J.-P. Delaboudinière, *et al.*, in *Proceedings of 10th European Solar Physics Meeting* (2002) ESA SP-506, p. 915.

Translated by A. Getling